

TITLE

*ASP Conference Series, Vol. **VOLUME**, **PUBLICATION YEAR***

EDITORS

Chandra–ASCA–RXTE observations of the micro-quasar GRS 1915+105

Julia C. Lee, Norbert S. Schulz

*MIT Center for Space Research, 77 Massachusetts Ave. NE80,
Cambridge, MA. 02139*

Christopher S. Reynolds

JILA - U. of Colorado, Campus Box 440, Boulder CO 80309

Andrew C. Fabian

Institute of Astronomy, Madingley Rd., Cambridge CB2 0HA U.K.

Eric G. Blackman

*Dept. of Physics & Astronomy, University of Rochester, Rochester, NY
14627*

Abstract. A *Chandra* AO1 30ks HETGS observation of the X-ray transient micro-quasar GRS 1915+105 reveals absorption edges and faint line emission over the HETG energy range. We find from a preliminary analysis evidence for prominent neutral K edges associated with iron, silicon, magnesium, and tentatively sulphur. The column densities assuming solar abundances are consistent with \sim few $\times 10^{22}$ cm $^{-2}$ in excess of the Galactic value, and may point to surrounding cold material associated with GRS 1915+105. Neutral $F_{K\alpha}$ emission, and ionized absorption from Fe XXV and Fe XXVI are resolved. We limit our discussion to the *Chandra* results.

1. Introduction

The X-ray transient GRS 1915+105 is an extremely energetic object in our Galaxy. Since its discovery by *Granat*/WATCH in 1992 (Castro-Tirado et al. 1992), it has shown repeated flares separated by short periods of quiescence. GRS 1915+105 has been studied extensively in multiple wavebands which include radio, infra-red and X-rays (e.g. see review by Zhang et al. 1997). In the X-ray band, its overall variability is extremely complex (possessing both regular and chaotic patterns) and challenges any current theoretical model. In its flaring state, the total (isotropic) luminosity can exceed 10^{39} erg s $^{-1}$, making it one of the most energetic objects known in the Galaxy. Since this exceeds the Eddington limit for a neutron star by almost an order of magnitude, it seems probable that this system contains a black hole. Given its distance of ~ 12.5 kpc (Mirabel & Rodríguez 1994) determined from the 21 cm absorption of atomic

hydrogen along the line of sight, and a visual extinction of $A_V \sim 27$, a direct optical determination of the mass function of this system is not possible – partly for this reason, the nature of the companion (i.e. LMXRB – e.g. Castro-Tirado et al. 1996 versus HMXRB – e.g. Chaty et al. 1996) is still debated. It is highly variable, with a luminosity which varies between a few $\times 10^{37} - 10^{39}$ erg s $^{-1}$, or in excess of this during the flaring state. One of the most remarkable aspects of this system is that X-ray flares are followed by superluminal ejection events which are observed in the radio band (Mirabel & Rodríguez 1994) – the inferred velocity of the jets (or more likely blobs) is $v \approx 0.9c$ (i.e. a Lorentz factor of 3), at an inclination $\approx 60 - 70^\circ$ to the line of sight. The Galactic binaries GRO 1655–40 and XTE J1748–288 display similar behavior. In this respect, these sources qualitatively resemble radio-loud active galactic nuclei (AGN) and are often called ‘micro-quasars’.

2. Observation

GRS 1915+105 was observed with the *Chandra* High Energy Transmission Grating (HETGS; Canizares et al., in preparation) on 2000 April 24 with a total integration time of ~ 31.4 ks (Fig. 1). Simultaneous *RXTE* observations were performed from 2000 April 24–25 with both the Proportional Counter Array (PCA) and High-Energy X-ray Timing Experiment (HEXTE) instruments. An *ASCA* target of opportunity (TOO) between 2000 April 19–25 also coincides with our *Chandra* observation. We concentrate only on the results of the *Chandra* observations for this proceeding.

The *Chandra* HETG is made up of the Medium Energy Grating (MEG) with a 2.5–31 Å (0.4–5 keV) bandpass, and High Energy Grating (HEG) with 1.2–14 Å (0.9–10 keV) bandpass. The peak resolving power ($E/\Delta E$) respectively for the MEG and HEG are 520 at 1 keV, and 1000 at 1 keV. The resolution of the higher orders improves by a factor of n for the n th order, but the spectral bandpass and efficiency are reduced accordingly.

Due to severe telemetry and photon pileup problems imposed by the large count rate of GRS 1915+105, the observation was performed using the *graded* telemetry mode, and a subarray which reduced CCD frametime by a factor of ~ 2 . Even though the source was at a relatively low state ($F_X = 9 \times 10^{-9}$ erg cm $^{-2}$ s $^{-1}$ which translates to $L_X = 2.14 \times 10^{38}$ erg s $^{-1}$; Fig. 1) during the epoch of our observation, we were nevertheless hampered by severe pileup in the HETG 1st orders. Because we were prepared for this eventuality, a ‘spatial window’ was used to block out the 0th order image (this would be completely piled-up even during periods of low flux for the energetics of GRS 1915+105.) However, because the 0th order position is crucial for defining an accurate wavelength scale, we calculate its position for our observation by fitting the intersection of the MEG and HEG dispersed images with the 0th order readout trace. The accuracy of such a technique for the determination of the 0th order position is $\sim 0.2 - 0.3$ pixels, which translates respectively to a wavelength accuracy of 0.002 Å and 0.004 Å, for the HEG and MEG 1st order.

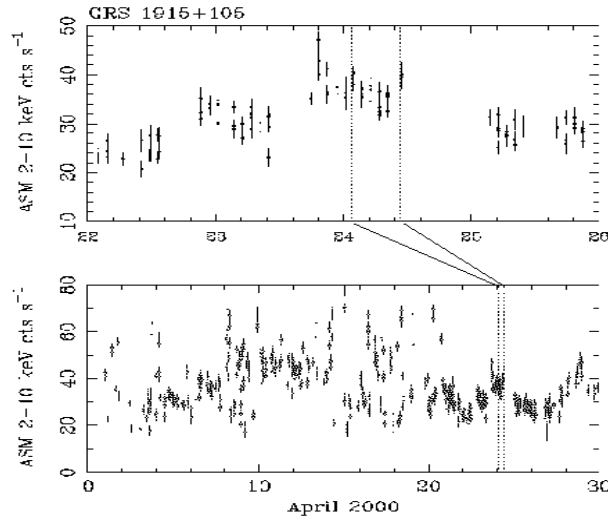


Figure 1. The *RXTE* All-Sky Monitor (ASM) light curve of GRS 1915+105 at the epoch of the *Chandra*-*ASCA*-*RXTE* observations. (The bottom light curve shows the behavior of GRS 1915+105 during the month of August 2000 for comparison.) Dotted vertical lines denote the period of the 31 ks *Chandra* observation. For comparison, 1 Crab ≈ 75 ASM $\text{cts s}^{-1} \approx 2 \times 10^{-8} \text{ erg cm}^{-2} \text{ s}^{-1}$.

PROMINENT SPECTRAL FEATURES SEEN IN THE TIME-AVERAGED DATA

Species	NEUTRAL FEATURES		
	λ_{mea} (Å)	${}^a\Delta\lambda$ (km s $^{-1}$)	${}^bN_{\text{H}}$ (10 22 cm $^{-2}$)
Mg K edge	9.52	-	2.7
Si K edge	6.74	-	3.5
S K edge	5.02	-	2.3
Fe K edge	1.74	-	10.0
Fe K α emission	1.94	1000	-
IONIZED FEATURES			
Fe XXV absorption	1.86	600	-
Fe XXVI absorption	1.78	1500	-

Table 1. a Velocity width (instrumental response removed). b Hydrogen column in excess of the Galactic ($1.76 \times 10^{22} \text{ cm}^{-2}$) value, assuming solar abundances.

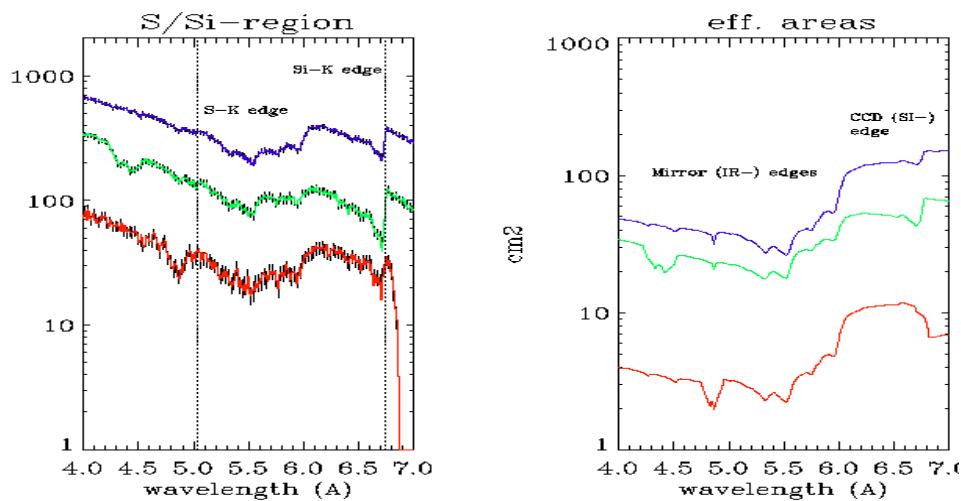
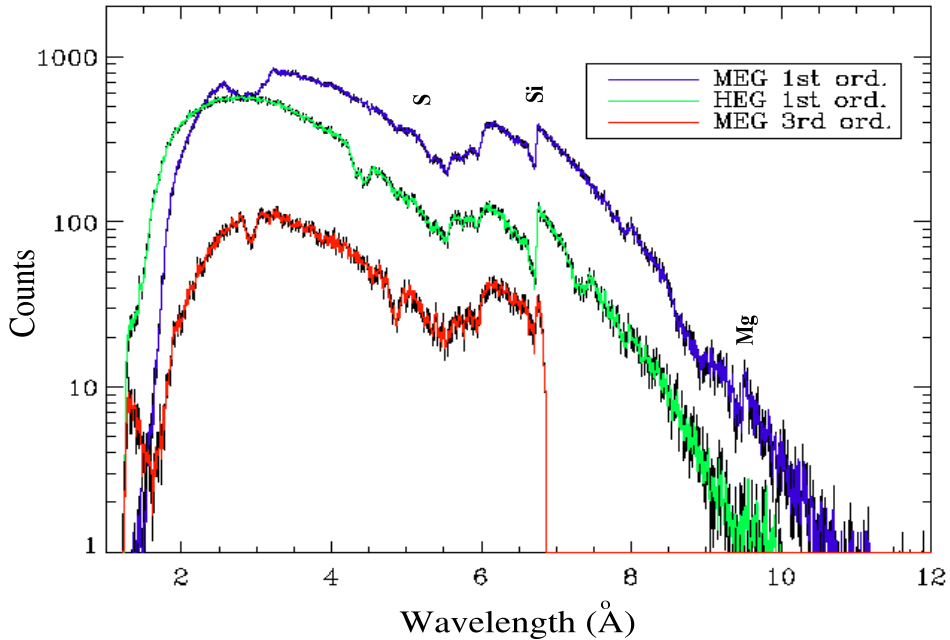


Figure 2. (Top) GRS 1915+105 count spectrum from top spectrum down : MEG 1st order, HEG 1st order, MEG 3rd order with three of the 4 neutral edges marked. (Bottom) The S-Si region is compared with the effective area curves for the detectors of interest (as in above plot scheme). Note the prominence of the Si edge in the MEG 3rd order spectrum where there is very little contribution from the detector edge.

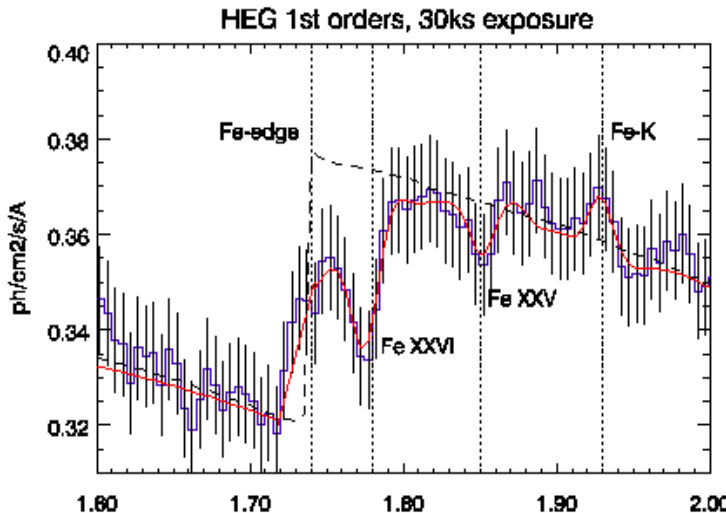


Figure 3. The iron region in the HEG band. Dotted lines represent the best fit continuum model. Neutral and ionized features are superposed on the continuum. The complete model (dashed lines which trace the spectrum) includes the continuum and absorption/emission features.

3. Cold and Ionized Material

We find evidence for prominent absorption edges due to iron, silicon, magnesium, and tentatively sulphur at the expected wavelengths for the neutral K-edges (Table 1, Figs. 2 and 3). The column in excess of Galactic ($1.76 \times 10^{22} \text{ cm}^{-2}$) determined from 21 cm absorption of atomic hydrogen along the line of sight) is calculated using the value for the K-shell photoionization cross section of the relevant species (Daltabuit & Cox 1972), and solar abundances. (We have used these abundances for comparison and acknowledge that there is no reason to prefer these abundances over interstellar abundances.) The validity of the Si edge is checked against the contribution from the *Chandra* CCDs - we find an upper limit of $\sim 20\%$ contamination from the detector to the depth of the edge. The validity that the Si edge is intrinsic to the source is reinforced in the MEG 3rd order spectrum (Fig. 2 bottom), where the edge remains prominent in the data, but for which there is a minute contribution from the detector. (The spectra for the relevant orders are the combined plus and minus sides; in the case of the MEG 3rd order, the Si edge seen in our spectrum for one of the sides fall on the backside (S1) chip where there is no/little contribution from the detector Si edge.)

In addition to neutral edges, neutral ($\text{Fe K}\alpha$) emission, and ionized iron (Fe XXV , Fe XXVI) resonant absorption features are superposed on the continuum (Fig. 3), at the expected wavelengths. The velocity widths and line wavelengths

of these features are detailed in Table 1. (The resolution of the *Chandra* HEG is $\sim 1600 \text{ km s}^{-1}$ at the iron energies. The values quoted in Table 1 already accounts for this.)

A first order approximation to the continuum is well fit by a simple Galactic absorbed cutoff power law of $\Gamma \sim 2$, and edges.

4. Summary

While analysis is still at its preliminary stages, we find definite evidence for N_H in excess of that expected from the Galactic column. This can be an abundance effect (i.e. interstellar abundances), or also likely cold material associated with GRS 1915+105. If the latter is true, our *Chandra* results would confirm reports from near-IR VLT observations of cold material associated with the source. Mirabel et al. (1996) suggested that heated dust is associated with the surroundings of GRS 1915+105. Additionally, Martí et al. (2000) have interpreted observed HI P-Cygni profiles in the near-IR which turn into blue emission wings when the system is in outburst, to be due to material which surrounds GRS 1915+105 that is blown out during an X-ray outburst. Our findings with *Chandra* for neutral spectral features are consistent with associated cold material in the environment of GRS 1915+105. The observed Doppler broadened iron emission and absorption features are likely to be from the disk or corona, or even possibly a wind.

References

Castro-Tirado, A. J., Brandt, S., & Lund, N., 1992, IAU Circ 599
 Castro-Tirado, A. J., Geballe, T.R., Lund N., 1996, ApJ, 461, L99
 Chaty, S., Mirabel, I. F., Duc, P. A., Wink, J. E., Rodríguez, L. F., A&A, 310, 825
 Daltabuit E., & Cox D.P., 1972, ApJ, 177, 855
 Martí, J., Mirabel, I.F., Chaty, S., Rodríguez, L.C., 2000, A&A, 356, 943
 Mirabel, I. F., & Rodríguez, L. F., 1994, Nature, 371, 46
 Zhang S. N., Mirabel I. F., Harmon, B. A., Kroeger, R. A., Rodríguez, L. F., Hjellming, R. M., Rupen, M. P., 1997 in 4th Compton Symposium